

Validation of the Underwater Synchronous Scanner Imaging Model

M. G. Gibby, J. H. Fahs, and M. B. Stine

Arion Systems, Inc.
8321 Old Court House Road, Suite 200
Vienna, Virginia 22182

Abstract - The Underwater Synchronous Scanner Imaging Model (USSIM) was developed as a software tool for exploring the design-trade space of the laser line scan system (LLSS). The critical software modules of USSIM have been subjected to a stressful validation process that relied on laboratory data collected with the LLSS. This validation effort demonstrated the utility of USSIM's predictive capabilities. This paper provides a description of the model and presents the results of the validation work.

I. INTRODUCTION

Underwater synchronous scanner imaging systems [1,2] have matured in the past few years to the point of providing high quality imagery in operationally attractive configurations. The advantages of scanning laser systems for underwater imaging were understood on a conceptual level as early as 1966 [3]. The first efforts to develop underwater synchronous scanners failed to achieve the expected performance. These designs were both operationally and economically unattractive [4]. The combination of a mature commercial technology base for critical system components, a focus on a mission appropriate for this imaging architecture, and system engineering responsive to these operational requirements contributed to the recent, successful developments.

This paper reports the results of an effort to validate the Underwater Synchronous Scanner Imaging Model (USSIM). USSIM was developed at ASI as an analytical tool to support the engineering development of the laser line scan system (LLSS). USSIM has been used to evaluate system designs and design modifications and to estimate system imaging performance in water conditions for which there is no operational experience. Recently, ASI, under contract to the Naval Coastal Systems Station, compared the model's performance estimates against experimental data that was collected by Spectrum Engineering with the LLSS in the Arctic Submarine Laboratory at the Naval Command, Control and Ocean Surveillance Center (NCCOSC) during the summer of 1991. This effort is the first systematic attempt to validate an underwater imaging model.

II. LASER LINE SCAN SYSTEM

Underwater cameras that use broad area illumination have short useful viewing distances (1 - 2 attenuation lengths) that result from the backscatter of the light source from

water column particulates. Synchronous scanning is an effective technique for suppressing the damaging effects of backscattered light. As shown in figure 1, the synchronous scanner generates an image of the scene by scanning the field-of-view (FOV) with a laser transmitter. The spot produced by the transmitter on the scene is tracked by an optical receiver with a narrow instantaneous field-of-view (IFOV). The photon flux entering the receiver is modulated by the scene reflectance. The image is created one pixel at a time by sampling the photo-electron current in the receiver's detector. The effective rejection of backscatter by the synchronous scanner is the consequence of the spatial separation of the transmitter and the receiver, the narrow transmitter beam and the small IFOV of the receiver. With this transmitter-receiver geometry, the transmitter overlaps the receiver's IFOV only at relatively long ranges, thereby, producing backscatter from a small and distant volume of water. The result is low levels of backscatter that permit viewing by the scanner at ranges (4 - 6 attenuation lengths) significantly greater than is possible with conventional cameras.

The range-gating technique [5,6] is also an effective method of rejecting backscatter. The long viewing ranges possible with range-gating make these systems attractive candidates for inspection missions. These systems due to the narrow FOV are less attractive as search systems. The synchronous scanner, in principle, has an important advantage in spatial resolution over both range-gated and conventional cameras systems. The resolution of these focal plane imaging systems is determined by the spatial response of the receiver; the resolution of the synchronous scanner is determined by the product of the spatial responses of the transmitter and receiver. This potential advantage of the synchronous scanner has not been realized in the design of the existing scanners.

The synchronous scanner has been implemented in two ways. The LLSS [1,2] sweeps a line across one dimension of the scene and depends upon the forward motion of the sensor platform to sweep out the scene in the orthogonal dimension. The LLSS concept shown in figure 1 is ideally suited to search operations where the forward motion of the search vehicle is needed to achieve high search rates. Two-dimensional scanners [7] that do not require vehicle motion to generate an image have been designed for inspection missions. USSIM is capable of computing imagery for either system architecture.

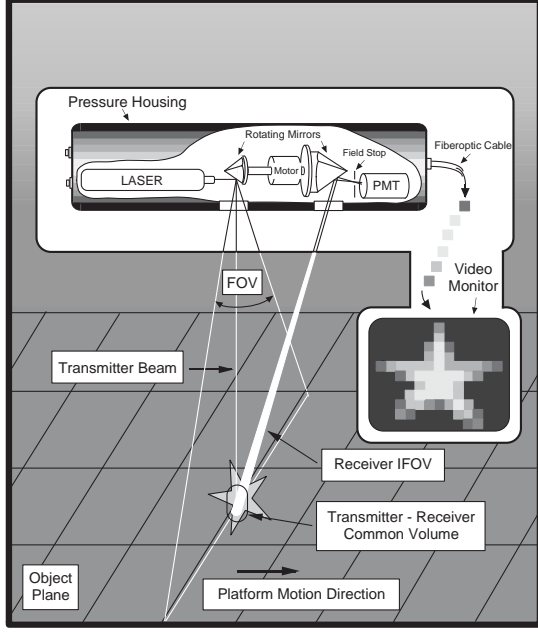


Figure 1. Laser line scan system.

III. UNDERWATER SYNCHRONOUS SCANNER IMAGING MODEL

USSIM is a linear systems model for incoherent imaging. This approach to modeling underwater imaging systems is described by Wells [8] and later by Mertens and Replogle [9]. The work of McGlamery [10] which is the basis for the UNCLES Model [11] is an adaptation of these concepts to camera systems. The focus of USSIM is synchronous scanning. Other imaging architectures, i.e., flying spot scanner and cameras, are special cases of synchronous scanning which makes USSIM readily adaptable to the analysis of these architectures. The backscatter model in USSIM is an adaptation of Replogle's [9]. USSIM computes the backscatter in range increments which enables analysis of range-gated systems. USSIM is implemented in a 32-bit FORTRAN and hosted on an IBM 486 computer.

USSIM is comprised of three principal software modules. The Image Module computes the transmitter power that is reflected off the scene into the photodetector of the receiver. The Backscatter Module calculates the transmitter power that is scattered by the medium into the photodetector without reflecting off the scene. The Detector Module accepts the optical power levels computed by the Image and Backscatter Modules and calculates for each sample of the scene the expected pixel level and pixel level variance. For objects in the scene, values of the display signal-to-noise ratio (SNR_d) statistic are computed. The Detector Module models the photodetector, signal processing, A/D converter, and display. The Detector Module is also capable of computing the effects of sensor platform motion on the SNR_d . The major functions of USSIM and their interrelationships are shown in figure 2. The Image and Backscatter Modules, which are the focus of this validation effort, are described in more detail in the following sections.

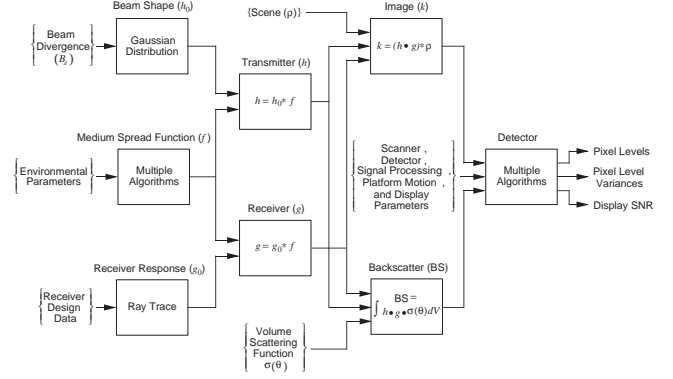


Figure 2. USSIM functional diagram.

A. Image Module

The Image Module calculates the fraction of transmitter power that is reflected off the scene and received at the photodetector using the following relationship.

$$k = (h * g) * \rho \quad (1)$$

where $*$ signifies a convolution operation. A derivation of this result is provided in [8]. $k(x, y)$ is the light power incident on the photodetector for a transmitter of unit power and a receiver that is directed at the point, (x, y) , in the scene. The scene is represented by $\rho(x, y)$ which is related to the diffuse reflectivity, $r(x, y)$, in the following way:

$$\rho(x, y) = \frac{r(x, y)}{\pi} \quad (2)$$

ρ represents that portion of power reflected from the point, (x, y) , in the scene into a differential solid angle about the normal direction. Equation (2) presumes a Lambertian reflector. The spatial response of the system, $h * g$, is the product of a transmitter part, h , and a receiver part, g , where the system includes the water column between the scanner and the scene. $h(x - x_o, y - y_o)$ is the irradiance distribution at the scene for a transmitter of unit power directed at the scene point, (x_o, y_o) . The effect of the medium is incorporated in h by convolving the normalized transmitter beam profile, $h_o(x - x_o, y - y_o)$, with the medium beam spread function (BSF), $f_b(x - x'_o, y - y'_o)$.

$$h = h_o * f_b \quad (3)$$

h_o is the irradiance distribution of a transmitter of unit power at the scene in the absence of scattering and absorption in the water column. $f_b(x - x'_o, y - y'_o)$ is the irradiance distribution of a beam of unit power that is focused to the point, (x'_o, y'_o) , in the scene. The spatial response of the receiver, $g(x - x_o, y - y_o)$, is the light power seen by the photodetector from a point source of unit radiant intensity located at (x, y) in the scene with the receiver directed at the scene point, (x_o, y_o) . The effect of the medium is also incorporated into g by convolving the receiver response in the absence of scattering and absorption processes in the water, $g_o(x - x_o, y - y_o)$, with the medium point spread function (PSF), $f_p(x - x'_o, y - y'_o)$.

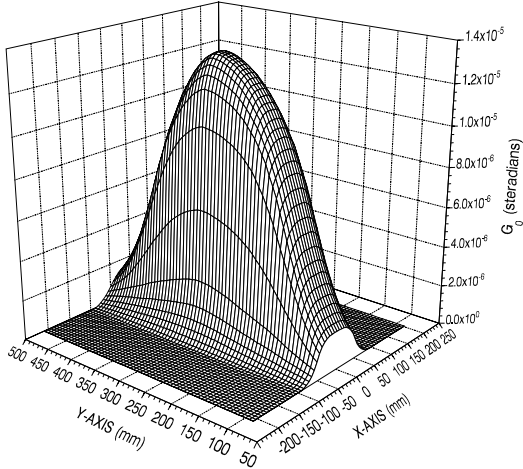


Figure 3. LLSS receiver response at a range of 36 feet for field stop settings of 2.45mm and 6.59 mm.

$$g = g_o * f_p. \quad (4)$$

g_o is obtained using a raytrace program that was written for this purpose. The design of the receiver optics is a critical input to the raytrace program. Figure 3 shows a typical g_o for the LLSS receiver design of figure 4. $f_p(x - x'_o, y - y'_o)$ is the apparent radiance distribution of a point source of unit radiant intensity located at the scene point, (x'_o, y'_o) .

The beam and point spread functions are important environmental inputs to the model. Wells [12] demonstrated the equivalency of these spread functions and Mertens and Replogle [9] identified the measurement conditions that must be satisfied for this equivalency to apply. USSIM exploits this equivalency and obtains the medium spread function, f , in one or more of the following ways.

- 1.) Measurement of f in the environment for which the model calculations are being performed.
- 2.) Application of the Duntley-Wilson empirical formula [13] to conditions where the scattering process can be adequately simulated by a particular class of artificial scattering agent.
- 3.) Application of small angle scattering theory [12,14] to obtain f from the volume scattering function, $\sigma(\theta)$, or to generate f at one range from an f that was obtained at another range.

B. Backscatter Module

The USSIM backscatter model is an adaptation of the Replogle model described in [8,9]. Backscatter is light from the transmitter that is scattered by the water column into the receiver via a path that does not encounter the scene. This model assumes that single, large-angle scattering events only contribute to backscatter. Multiple, large-angle scattering events are ignored. The effects of multiple, small-angle scattering events are incorporated by means of the medium spread function. The Backscatter Module performs the following integration numerically.

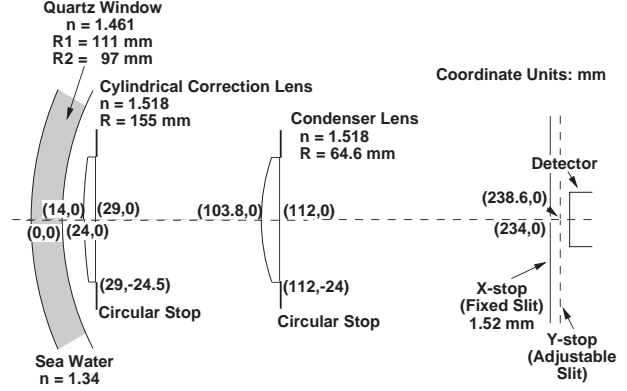


Figure 4. An equivalent diagram of LLSS receiver optics.

$$B_s(R) = \int_0^R \int_{-\infty}^{\infty} \int_{-\infty}^{\infty} \sigma(\theta) h(x, y, z) g(x, y, z) dx dy dz \quad (5)$$

where the dependence of h and g on z , the coordinate perpendicular to the scene, is made explicit. $B_s(R)$ is the backscatter power resulting from scattering in the water located between the $z=0$ plane and the scene in the $z=R$ plane. θ is the scattering angle associated with the large-angle scattering event. $B_s(R)$ is calculated as a sequence of two-dimensional integrals over planes of constant z .

IV. EXPERIMENTAL APPROACH AND DATA REDUCTION

All measurements were made in the Arctic Submarine Laboratory's stainless steel tank with dimensions, 105 ft x 28 ft x 4 ft. The tank is crossed by a moveable bridge which provided the platform for deploying the targets and the photomultiplier tube (PMT) that was used to measure the beam spread functions. The scanner was located at one end of the tank with its axis of symmetry vertical and optical window oriented towards the bridge. This produced a horizontal scan line that cut across the vertically oriented bars of the targets. To make the tank appear larger than its dimensions, black felt cloth was placed on the floor and back walls of the tank and was also floated on the surface of the water. In an attempt to detect edge effects, beam spread functions were measured at PMT depths of 1, 2, and 3 feet. The BSFs obtained at the three depths were identical.

The tank was cleaned and filled with San Diego tap water with a high volume attenuation coefficient, $\alpha \sim 0.5 \text{ m}^{-1}$, that dropped with time. The first set of experiments were performed in this water with the $\alpha = 0.364 - 0.381 \text{ m}^{-1}$. The water was then filtered for several days until an $\alpha \sim 0.05 \text{ m}^{-1}$ was achieved. Artificial scattering agent (Maalox) was used to bring the α to 0.118 m^{-1} where another set of measurements was taken. The same scattering agent was again added to bring the α to the 0.220 m^{-1} range for the final set of measurements. During all of these measurements, α tended to drift with time. During the last set of measurements, some scattering agent was added to maintain α in the desired range. α was measured coincident with each experimental data set.

Two types of targets were used for these measurements - a set of black and white bar charts with different bar widths and a 7-level gray scale with bars 6-inches wide. Only data on the bar charts are presented in this report. The stripe widths (half-period) on the bar charts were 4, 2, 1, 0.5, 0.25, and 0.125 inches. The in-water reflectances of the white and black stripes of the bar chart were estimated to be 0.864 and 0.018 respectively. The LLSS target data was acquired with a Nicolet digital scope. The waveform data and the LLSS log files which recorded the relevant LLSS settings were provided to ASI on magnetic disks. This data along with the PMT and laser calibration data provided the information needed to reduce the voltage levels at the output of the LLSS preamplifier to optical power levels at the input to the PMT. The power levels were normalized to 1W of transmitter power. These results were compared with the combined outputs of the Image and Backscatter Modules.

The backscatter measurements provided an independent validation of the Backscatter Module. This data was taken by removing the target from the tank and stopping the LLSS scan motor with the laser directed down the middle of the tank. The upper and lower variable field stops were set for a small opening of more or less fixed size. The field stops were moved in a succession of steps from viewing the near field to the far field. At each step, the backscatter power incident on the detector was measured. The backscatter data was reduced to an optical power density curve, i.e., a plot of power per unit of field stop opening as a function of the position of the opening. The backscatter power density is integrated between the two field stop positions to obtain an estimate for the measured backscatter associated with these field stop settings.

Beam spread functions were measured by deploying a PMT packaged in a waterproof housing from the bridge of the tank. The laser transmitter was scanned slowly and repetitively across the PMT. The depth of the PMT was adjusted until its response to the laser beam was maximized. With the appropriate equipment calibration data, the signal waveform was reduced to the optical irradiance distribution of a BSF.

V. RESULTS

This validation effort focused on USSIM's ability to predict light power levels observed by the LLSS. The LLSS backscatter measurements provided a means of validating the Backscatter Module independent of the Image Module. As a result of the validation work on the Backscatter Module, a consistent procedure was developed to estimate the backscatter component in LLSS image data. By removing this component from the image data, a separate check of the predictions of the Image Module was also made. The LLSS image data provides the basis for validating the sum of the outputs of the Backscatter and Image Modules.

A. Backscatter Module

Table I summarizes the results of the backscatter measurements and a set of USSIM backscatter calculations. The

TABLE I
COMPARISON OF CALCULATED AND MEASURED
BACKSCATTER OPTICAL POWER LEVELS

Alpha (m ⁻¹)	Range [†] (ft)	Measured (W)	Ratio [‡]			
			Measured BSF	Duntley-Wilson BSF		
				$\alpha/a=4$	$\alpha/a=2$	$\alpha/a=4$
0.381	18.0	1.13×10^{-8}	0.45	0.31	0.44	0.49
	36.0	1.12×10^{-9}	0.58	0.20	0.45	0.69
	45.0	2.34×10^{-9}	0.38	0.19	0.42	0.61
0.212	27.1	4.71×10^{-10}	1.32	1.04	1.33	1.38
	54.9	9.36×10^{-10}	1.46	0.74	1.10	1.27
	73.5	7.37×10^{-10}	1.56	0.60	1.00	1.28
0.114	54.7	1.00×10^{-9}	2.03	1.54	1.91	2.04
	97.0	4.49×10^{-10}	2.43	1.49	1.97	2.21

[†] Range indicates LLSS field stop settings used for image data; both measured and calculated backscatter were actually acquired for the full length of the tank (98 feet).

[‡] Ratio = Calculated Power/Measured Power.

table provides values of the measured backscatter and ratios of the calculated to measured backscatter. The ratios are provided for calculations performed with the measured BSFs and BSFs obtained using the Duntley-Wilson formula [13]. The range values in the table indicate that the estimates of backscatter, measured and calculated, were obtained for the same field stop settings that were used to obtain target data at these ranges. The backscatter measurements were taken with an unobstructed view of the tank and the calculations were performed out to 98 feet to mimic the measurement conditions. The calculated results in the table for the measured BSFs assume an $\alpha/a=4$ for the purpose of determining the value of the volume scattering function, $\sigma(\theta)$. $\sigma(\theta)$ for the artificial scattering agent [17] was used for all calculations.

The most striking trend of the table is the apparent dependence of the ratio on α . The calculated results obtained with measured BSFs appear to be low by a factor of two in the high α water and high by a factor of two in the low α water. To provide more insight into the difference between the measured and these calculated results, backscatter calculations were performed for additional field stop settings for the 4 m water case. These results which are summarized in figure 5 show significantly better agreement for the large field stop settings. These settings correspond to short viewing ranges. This tendency for the results to diverge for longer viewing ranges suggested the possibility of an error in the measurement of α . Additional backscatter calculations for differing values of α indicated that values of α resulting in agreement at the longer range settings produced disagreement at the shorter range settings. Thus, α measurement error does not appear to explain the observed differences.

Consideration was given to the following potential sources of computational and measurement errors: 1.) choice of α/a , 2.) use of $\sigma(\theta)$ for artificial scattering

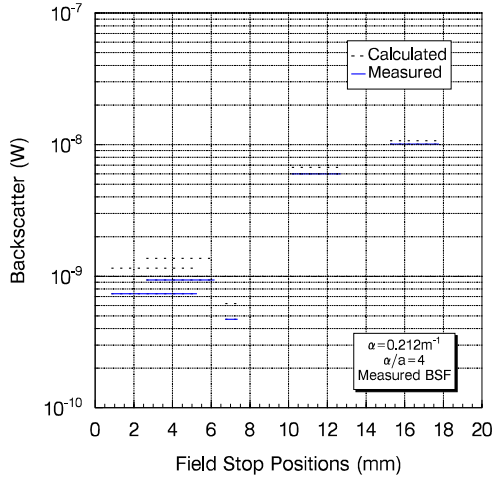


Figure 5. Comparison of calculated and measured backscatter as a function of field stop positions.

agent, 3.) edge effects of the tank, and 4.) problems with the measurement of the BSF. As shown by the calculated results obtained with the Duntley-Wilson BSFs, the backscatter is sensitive to α/a . This sensitivity is due mainly to the spreading of the BSF with increasing α/a that results in a greater common volume. The effect on the backscatter through $\sigma(\theta)$ is less significant. Thus, α/a alone will not explain the trend for the calculated results obtained using measured BSFs. The scattering in the 8 m and 4 m waters was due to artificial scattering agent; thus, using $\sigma(\theta)$ for the artificial scattering agent is appropriate for these cases. Analysis of the measurement geometry, the receiver IFOV, and ranges at which the model predicted significant backscatter indicated that tank edge effects should not have been a significant factor. The problem with the calculated results using measured BSFs appears to lie with the BSFs. The measured BSF in the 8 m water was compared to BSFs generated by the Duntley-Wilson formula for various values of α/a . The measured BSF suggested a value of 6 or greater when a value closer to 2 was expected based on the work of Petzold [17]. Petzold employed the same filtering process that was used to prepare the water for these experiments and determined that the volume attenuation after filtering was due almost exclusively to absorption. Doubling the α with scattering agent should have produced $\alpha/a \approx 2$. The calculations using Duntley-Wilson BSFs for $\alpha/a=2$ resulted in ratios of 1.5 for both ranges (54.7 and 97.0 feet) in the 8 m water. The source of this potential problem with the BSF measurement has not been resolved. The shaded regions of Table I for the 8 m and 4 m water cases represents results for the best estimates of water conditions based on [17]. These results show significantly better agreement than the corresponding results based on the measured BSF.

B. Image Module

The Image Module calculates the optical power level at the detector for that component of incident light that is

reflected off the target. Any measurement of this component of the incident light will be contaminated with backscatter. The section of Table II labelled, “Without Backscatter,” summarizes the comparison of Image Module calculations with measured image data that is modified by subtracting the backscatter component. The backscatter component is estimated using the measured backscatter and adjusting the measured value to correspond to the particular target range and to small changes in α . These adjustments to the measured backscatter were made based on model calculations of the backscatter for the conditions of the backscatter and image measurements. The image data of Table II is for the 4-inch bar chart target. This wide stripe data was used to eliminate any ambiguities in the data that might be associated with the small but unknown transmitter beamwidth. The optical power levels shown in the table are sampled at the mid-point of the black and white stripes.

Compared to the backscatter results of Table I, the image data exhibits no apparent trend with α . However, the low ratio values for the San Diego tap water ($\alpha=0.364 \text{ m}^{-1}$) are consistent with and similar in magnitude to the backscatter results in the same water. The ratio values run from 0.23 to 1.34. The calculated results of Table II are based on measured BSFs.

C. Combined Image and Backscatter Modules

The section of Table II labelled, “With Backscatter,” summarizes the comparison of the measured target data with the combined results of Image and Backscatter Module calculations. As might be expected, combining the power level estimates removes some of the extreme variability that is observed in the separate data sets. The major trends remain. The ratios for the 0.364 m^{-1} water are the most extreme in the 0.25 to 0.35 range. All other results are within a factor of 2 of the measured result.

VI. CONCLUSIONS

The results of comparing measured and calculated optical power levels demonstrated generally credible agreement between theory and experiment. Some significant differences in the measured and calculated results have not been resolved. Two apparently significant trends in the data are not well understood - the apparent increase in the backscatter ratio values with decreasing α and the low ratio values for backscatter and image data for the 0.364 m^{-1} water case. This validation effort would have benefited by an unambiguous measurement of the optical properties of the water.

Under the assumption that the observed differences between the calculated and measured results are due to failings of the model, the predictive properties of USSIM are still quite good. For example, it can be shown that for the worst case of the 0.364 m^{-1} water USSIM will predict the range at which the system achieves a level of performance within 0.3 attenuation lengths of the range that the performance level will actually be observed.

TABLE II
COMPARISON OF CALCULATED AND MEASURED OPTICAL POWER LEVELS FOR 4-INCH BAR TARGET †

Alpha (m ⁻¹)	Range (ft)	Without Backscatter				With Backscatter			
		White		Black		White		Black	
		Measured	Ratio‡	Measured	Ratio‡	Measured	Ratio‡	Measured	Ratio‡
0.364	18.0	1.40∞10 ⁻⁶	0.34	6.06∞10 ⁻⁸	0.23	1.41∞10 ⁻⁶	0.34	6.68∞10 ⁻⁸	0.25
	35.0	9.77∞10 ⁻⁹	0.33	2.15∞10 ⁻⁹	0.32	1.09∞10 ⁻⁸	0.35	3.27∞10 ⁻⁹	0.35
	45.0	1.86∞10 ⁻⁹	0.36	8.73∞10 ⁻¹⁰	0.28	4.33∞10 ⁻⁹	0.35	3.34∞10 ⁻⁹	0.32
0.222	27.1	2.33∞10 ⁻⁸	1.34	2.68∞10 ⁻⁹	0.55	2.34∞10 ⁻⁸	1.34	2.83∞10 ⁻⁹	0.60
0.269	54.9	8.60∞10 ⁻¹⁰	0.73	3.32∞10 ⁻¹⁰	0.87	1.42∞10 ⁻⁹	0.90	8.96∞10 ⁻¹⁰	1.04
0.221	67.4	8.18∞10 ⁻¹⁰	0.49	3.29∞10 ⁻¹⁰	0.60	1.51∞10 ⁻⁹	0.95	1.02∞10 ⁻⁹	1.21
0.117	54.7	8.34∞10 ⁻⁸	0.53	5.03∞10 ⁻⁹	1.08	8.41∞10 ⁻⁸	0.54	5.74∞10 ⁻⁹	1.20
0.113	97.0	3.01∞10 ⁻⁹	0.52	4.81∞10 ⁻¹⁰	1.03	3.47∞10 ⁻⁹	0.74	9.37∞10 ⁻¹⁰	1.61

† $\sigma(\theta)$ for $\alpha/a = 4$ assumed.

‡ Ratio=Calculated Power/Measured Power.

ACKNOWLEDGMENTS

M.G.G. would like to thank Dr. Bryan W. Coles of Applied Remote Technology and Dr. Michael P. Strand of the Naval Coastal Systems Station for their encouragement of this model development. The authors would also like to thank Dr. Coles and the former engineering staff of Spectrum Engineering for their support in providing the data on which this validation work is based.

REFERENCES

- [1] Leatham, J. and B. W. Coles, "Use of Laser Sensors for Search and Survey," *Underwater Intervention '93 Conference Proceedings*, pp. 171-186, 1993.
- [2] Gordon, A., "Underwater Laser Line Scan Technology," *Underwater Intervention '93 Conference Proceedings*, pp. 164-170, 1993.
- [3] Angelbeck, A. W., "Application of a Laser Scanning and Imaging System to Underwater Viewing," *SPIE Underwater Photo-Optics Seminar Proceedings*, 1966.
- [4] Heckman, P. J. and P. D. McCardell, "A Real-time Optical Mapping System," *SPIE Proceedings*, vol. 160, pp. 189-196, 1978.
- [5] Heckman, P. J., "Underwater Range Gated Photography," *SPIE Underwater Photo-Optics Seminar Proceedings*, 1966.
- [6] Swartz, B. A., "Diver and ROV Deployable Laser Range Gate Underwater Imaging Systems," *Underwater Intervention '93 Conference Proceedings*, pp. 193-198, 1993.
- [7] Kulp, T. J., D. Garvis, and R. Kennedy, "Current Status of the NAVSEA Synchronous Scanning Laser-imaging System," *SPIE Proceedings*, vol. 980, pp. 57-65, 1988.
- [8] Wells, W. H., "Medium and System Transform Functions," AGARD Lecture Series No. 61, *Optics of the Sea*, Session 4.3, 1973. (Obtainable from Report Distribution Unit, NASA, Langley, Virginia)
- [9] Mertens, L. E. and F. S. Replogle, Jr., "Use of Point Spread and Beam Spread Functions for Analysis of Imaging Systems in Water," *J. Opt. Soc. Am.*, vol. 67, pp. 1105-1117, 1977.
- [10] McGlamery, B. L., "A Computer Model for Underwater Camera Systems," *SPIE Proceedings on Ocean Optics VI*, vol. 208, pp. 221-232, 1979.
- [11] Jaffe, J. S. and C. Dunn, "A Model-Based Comparison of Underwater Imaging Systems," *SPIE Proceedings on Ocean Optics IX*, vol. 925, 1988.
- [12] Wells, W. H., "Theory of Small Angle Scattering," AGARD Lecture Series No. 61, *Optics of the Sea*, Session 3.3, 1973. (Obtainable from Report Distribution Unit, NASA, Langley, Virginia)
- [13] Wilson, W. H., "Underwater Lighting by Low Coherence Sources," Ph.D. Dissertation, University of California, San Diego, 1972.
- [14] Wells, W. H., "Loss of Resolution in Water as a Result of Multiple Small-angle Scattering," *J. Opt. Soc. Am.*, vol. 59, pp. 686-691, 1969.
- [15] Beaton, R. J., R. W. Monty, and H.L. Snyder, "An Evaluation of System Quality Metrics for Hard-Copy and Soft-Copy Displays of Digital Imagery," *SPIE Proceedings on Applications of Digital Image Processing VI*, vol. 432, 1983.
- [16] Rosell, F. A., and R. H. Wilson, "Recent Psychophysical Experiments and the Display Signal-to-Noise Ratio Concept," Chapter 5, *Perception of Displayed Information*, Edited by Lucien M. Biberman, Plenum Press, New York, 1973.
- [17] Petzold, T. J., "Volume Scattering Functions for Selected Ocean Waters," *Scripps Institution of Oceanography Report 72-78*, 1972.